Spread of Matter over a Neutron-Star Surface During Disk Accretion: Deceleration of Rapid Rotation

N.A. Inogamov[1,2] and R.A. Sunyaev[2,3]

[1]*Landau Institute for Theoretical Physics, RAS, Chernogolovka, 142432, Russian Federation*
[2]*Max-Planck Institut fuer Astrophysik, Garching, D-85741, Germany*
[3]*Space Research Institute, RAS, Moscow, 117997, Russian Federation*

The problem of disk accretion onto the surface of a neutron star with a weak magnetic field at a luminosity exceeding several percent of Eddington is reduced to the problem of the braking of a hypersonic flow with a velocity that is 0.4-0.5 of the speed of light above the base of the spreading layer – a dense atmosphere made up of previously fallen matter. We show that turbulent braking in the Prandtl-Karman model with universally accepted coefficients for terrestrial conditions and laboratory experiments and a ladder of interacting gravity waves in a stratified quasi-exponential atmosphere at standard Richardson numbers lead to a spin-up of the massive zone that extends to the ocean made up of a plasma with degenerate electrons. Turbulent braking in the ocean at the boundary with the outer solid crust reduces the rotation velocity to the solid-body rotation velocity of the star. This situation should lead to strong heating of deep atmospheric layers and to the switch-off of the explosive helium burning mechanism. Obviously, a more efficient mechanism for the dissipation of a fast azimuthal flow in the atmosphere should operate in X-ray bursters. We show that a giant solitary gravity wave in the atmosphere can lead to energy dissipation and to a sharp decrease in azimuthal velocity in fairly rarefied atmospheric layers above the zone of explosive helium burning nuclear reactions. We discuss the reasons why this wave, that has no direct analog in the Earth's atmosphere or ocean, appears and its stability. We pose the question as to whether neutron stars with massive atmospheres, spun up to high velocities by accreting matter from a disk, can exist among the observed Galactic X-ray sources.

INTRODUCTION

The problem of a boundary layer under disk accretion onto a neutron star (NS) with a weak ($< 10^8$ G) magnetic field arose from the necessity of interpreting the observations of X-ray sources in low-mass binaries with neutron stars. In particular, we are talking about X-ray bursters called so because of recurrent X-ray bursts (Lewin et al. 1993). These bursts result from thermonuclear explosions in the matter that fell onto the NS after a preceding burst. The very interesting physical problem of a flow in a boundary layer has no analogs in the Earths atmosphere and is inaccessible to modeling under laboratory conditions. It is reduced to the problem of inflow from a disk, braking, settling, and redistribution of the accreting matter along the meridian on the NS surface. On the NS, this matter forms a powerful flow that rotates azimuthally with a hypersonic velocity relative to the surface (the accretion rate is $10^{16} - 10^{18}$ g s^{-1}). The flow is in the shape of an equatorial belt that moves with a velocity slightly less than the Keplerian one ($\sim 40 - 50\%$ of the speed of light) above a compact star with a radius of ≈ 10 km. In this case, the acceleration due to gravity $g_{grav} = GM/R^2 = 10^{14}$ cm s^{-2}, which

(along with the plasma temperature of the order of several keV) determines the pressure scale height $\sim 0.1 - 1$ m, exceeds the familiar terrestrial one by eleven orders of magnitude. The flow velocity is close to 120000 km s^{-1}, i.e., it exceeds the speed of sound and the velocities of any motions in the Earths atmosphere by five orders of magnitude. It exceeds even the parabolic velocity on the Earths surface and, hence, the velocity of the rockets that place interplanetary vehicles in orbit by four orders of magnitude. Even the fastest asteroids and comets had velocities lower by thousands of times during their entry into the Earths atmosphere.

The Levitating Layer

In our previous paper (Inogamov and Sunyaev 1999; below referred to as IS99 for short), we suggested solving this problem in the 1D approximation by reducing it to the problem of the spreading of a thin layer of rapidly rotating matter over the NS surface (Fig. 1). We assumed that the main friction took place in an even thinner base of the spreading layer and the picture is similar to the braking of a supersonic flow near a wall. This picture had its fairly unexpected consequences. The energy release during the braking of such a flow is so great that the local radiation flux per unit surface area is close to the Eddington value, $q_{Edd} = L_{Edd}/4\pi R^2 = m_p g_{grav} c/\sigma_T \sim 10^{25}$
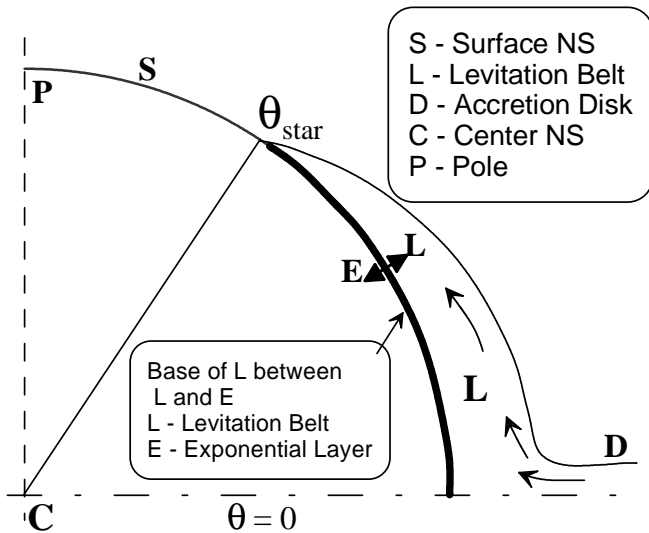
FIG. 1: Accretion of matter from the disk D into the spreading layer L. In the spreading layer or belt, the matter levitates (the letter L on the arrow LE). The base is indicated by the thick arc extending from the equator $\theta = 0$ to latitude $\theta_\star$. This is the zone of contact between the layer L and the neutron star. It bounds the belt L from below. In the base of the belt L and under it, the density ρ grows quasi-exponentially. This is indicated by the letter E (Exponential) on the arrow LE. This growth continues up to the boundary between the exponential atmosphere and the ocean that forms a layer of degenerate fluid above the solid NS crust surface. The NS surface is denoted by the letter S; C and P are the NS center and pole.

erg s^{-1} cm^{-2}, while the radiation pressure force in the flow zone easily compensates for the difference between the force of gravity and the centrifugal force. As a result, the effective acceleration due to gravity determined by the combined action of these three forces works. Accordingly, the pressure scale height ~ 1 km increases sharply compared to $\sim 0.1 - 1$ m (in the absence of a powerful radiation flux and rapid rotation) and the latitudinal flow levitates above the stellar surface.

The meridional component of the centrifugal force is directed toward the equator. It prevents the latitudinal flow from expanding along the stellar meridian. The flow expansion along the meridian is possible only through the loss of angular momentum due to friction on the wall and the corresponding decrease in the meridional component of the centrifugal force (see Section 2.8). The height of the levitating layer decreases as one recedes from the equator. Thus, the meridional pressure gradient maintains the poleward spreading of the matter (losing its angular momentum) along the meridian (Fig. 1).

The upper boundary of the spreading layer along the meridian $\theta_\star$ shown in Fig. 1 is determined by the area on which the energy release due to flow braking can provide a nearly Eddington radiation flux per unit surface area and levitation with a high speed of sound and a
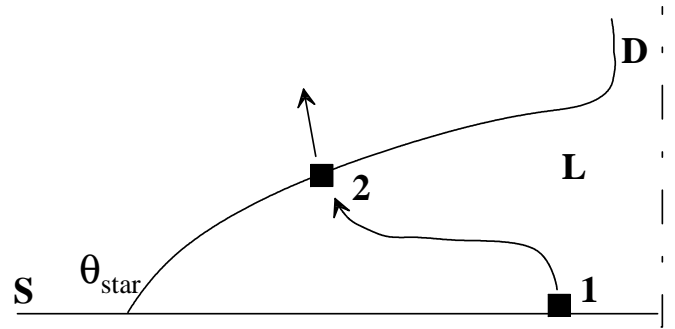

FIG. 2: Hydrodynamic advection of photons along the meridian poleward. Radiation is transported by the spreading layer from point 1 to point 2 along the track $1 \rightarrow 2$ with energy radiated away from the surface of the levitating belt L at point 2 (see IS99). In contrast to the previous Figure, the stellar boundary S is indicated here by the straight line and is placed horizontally.

fairly large pressure scale height. The IS99 solution predicts the presence of two equidistant (from the equator) latitude bands with the Eddington surface brightness in X-rays on the surface of an accreting NS. The distance from the bright bands to the equator and their width increase with accretion rate. The levitating belt covers the entire stellar surface at an Eddington accretion rate $\dot{M} \approx 2 \times 10^{18}$ g s^{-1}. The low surface brightness near the equator is related to an infinitesimal effective gravity due to the closeness of the flow velocity to its Keplerian value. The advection of radiation energy (hydrodynamic heat transport) contributes to the removal of the energy (being released in the equatorial zone) to higher latitudes. The scheme for advective photon transport is shown in Fig. 2. The advection of radiative energy is responsible for the formation of the mentioned bright bands.

The IS99 solutions were based on the conclusion by Popham and Sunyaev (2001) about the presence of a thin neck in the accretion disk D at the place of mass transfer from the disk into the spreading layer L (see Fig. 1). This disk thinning at the inner boundary (the diskboundary layer boundary) is a natural consequence of the angular momentum conservation law (for a discussion, see Shakura and Sunyaev 1973).

The Base of the Spreading Layer

In this paper, we made an attempt to calculate the structure of the "sole" or the base of the levitating layer in which (a) the flow brakes, (b) the main energy release takes place, and (c) the accreting matter settles (the base is the arc $0 < \theta < \theta_\star$ of circumference S in Fig. 1). We hoped to get the picture of a thin sublayer near the NS surface that would confirm the assumptions made when deriving the IS99 equations. Below in this section, we briefly summarize the results of our attempts to find a so-

lution of the problem that leads to an efficient braking of the flow under consideration. The solution was sought in the context of a well-known approach to turbulent viscosity well studied in nature and numerous experiments. We are talking about the Prandtl-Karman model of turbulent friction (Schlichting 1965). In addition, for checking we used the second approach with α-friction suggested by Shakura and Sunyaev (1973) for accretion disks.

Here, we will consider in detail the physical processes in an axisymmetric flow that take place in a narrow (along the meridian) column of matter (a "pipe"; see Section 1.10 and Fig. 19 below) under the levitating layer. This approximation is valid, because the column height is small compared to the extent of the base along the meridian. Attention will be focused on the decrease in the azimuthal velocity of the matter in this column and on the change in radiation flux and matter temperature with depth or, which is more convenient, with surface density Σ of matter between the point of interest to us at a given depth and the lower boundary LA of the levitating layer (see Fig. 3). Obviously, the concept of a solid wall is absent in our formulation of the problem – the flow of rarefied matter in the levitating layer L rushes above the atmosphere made up of the plasma that left this layer slightly earlier.

The settling of matter into the base from the levitating layer. In IS99, we neglected the settling of matter from the levitating layer L, because this layer spread above an impermeable wall. According to this simplest picture, all of the accreting matter from the disk was transported along a spiral (the rotation plus the motion along the meridian) to the shock wave at the boundary $\theta_\star$ of the layer L (see Figs. 1 and 2). Beyond the latitude $\theta_\star$ $(\theta > \theta_\star)$, levitation ceases and the cold matter passed into corotation with the star spreads poleward. According to IS99, this corotating matter fills the entire NS surface and, in particular, forms the underlying envelopes beneath the belt L.

In this paper (for the equations and a detailed discussion of the solution, see Sections 3–8), we take into account the settling of matter inside the levitating belt L. The settling rate is specified by the function $\dot{\Sigma}(\theta)$. It characterizes the settling in the vertical column of the latitude ring at various angular distances θ from the equator. Allowance for $\dot{\Sigma}(\theta)$ gives rise to the term in the angular momentum equation responsible for the radial advection of angular momentum $\propto \dot{\Sigma}(\theta)v_\varphi$ (see Section 4.1). Similarly, such advection enters into the energy equation.

The settling rate $\dot{\Sigma}$ is low near the equator (where the rotation velocity of the matter in the levitating flow is nearly Keplerian) and is comparable to the advection rate upward along the meridian near the surface brightness maxima (above, we have already mentioned the existence of two bright latitude bands predicted in IS99). To calculate $\dot{\Sigma}(\theta)$ at fixed latitude θ, in Section 6.5 we
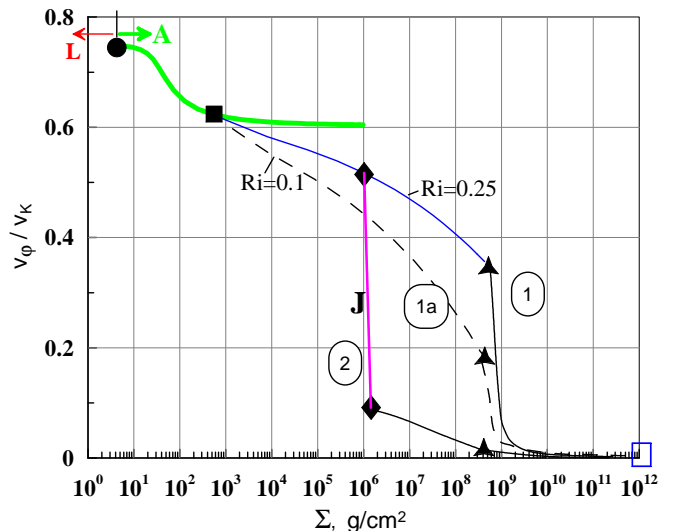

FIG. 3: Rotation velocity profile as a function of column density Σ. Here, Σ is measured from the horizon LA where matter is balancing on the verge of a wind; L denotes the levitating layer; A is the upper part of the base; and LA is the boundary between the layers L and A. It is highlighted by the filled circle. The layer L is to the left of this circle, see arrows in the figure. The profiles with labels Ri =0.25 and 0.1 refer to the standard (0.25) and reduced (0.1) values of the Richardson number, which is equal to the square of the ratio of the gravitational and shear frequencies. One can see that even in the case with reduced Ri-number (Ri=0.1) the gravity stratification strongly decreases the exchange of momentum due to shear turbulence. This gives maximal decrease of v_φ with depth. The decrease in velocity v_φ between the filled circle and square is related to turbulent shear friction according to the Prandtl-Karman model (see Section 1.3). The gravity wave ladder is located between the filled square and triangle. In case 2, the existence of a giant gravity wave is assumed (see Section 1). It reduces sharply the velocity v_φ from one diamond to another (velocity jump J). In cases 1 and 1a, the velocity v_φ gradually decreases in the exponential atmosphere between the filled square and triangle. Unless the rapid rotation is terminated by the jump J, very dense and massive layers fall into rotation with high frequencies. The triangle corresponds to the helium flash ignition horizon; the ocean of degenerate fluid begins under it. The ocean occupies the layer between the triangle and the open square (this is the upper boundary of the solid crust).

use the condition for the transition to a state of levitation at the boundary between the belt L and the base. The force stresses related to turbulent friction and nonlinear interaction in the gravity wave ladder are responsible for the braking of Keplerian rotation.

Difficulties with the standard approach to the problem suggesting the flow braking in a thin base through turbulent viscosity. A detailed analysis (see Sections 1.3 and 8 in the full paper) showed that the simple solution with a thin base and a gradual transition (see Fig. 1, the arrow L → E) from rapid rotation in the levitating belt L to slow NS rotation is possible, but it

imposes stringent requirements on the viscosity parameters in this base. These requirements are in conflict with the available experimental data on viscosity in near-wall supersonic flows.

The solution with a smooth rotation velocity profile $v_\varphi(r)$ in which the velocity v_φ decreases to the NS rotation velocity through turbulent viscosity exists only when the viscosity coefficient in the Prandtl-Karman model is chosen to be hundreds of times less than its universally accepted value (see Section 8). Likewise, the α-coefficient in the Shakura-Sunyaev (1973) model of viscous stress should be 10^{-3} at the speed of sound including the radiation pressure or 10^{-2} if the thermal ion velocity is substituted into the formula for α (see Section 11.2).

Velocity distributions for different viscosities are shown in Figs. 4-6. They describe the decrease of v_φ in the upper part of zone A shown in Fig. 3 by the thick curve which starts from the point LA and goes down in depth. The thick curve in Fig. 3 corresponds to the part of the zone A where the velocity shear dominates the flow. Here oscillations due to gravity waves are suppressed since the Richardson number

$$\mathrm{Ri} = N^2/\omega_{sh}^2$$

is small: $\mathrm{Ri} \ll 1$; N and ω_{sh} - are the Brunt-Väisälä and shear frequencies.

A situation with the critical Richardson number $\mathrm{Ri} \approx 0.25$ is shown in Fig. 7. Discussion of the critical value may be found in Kippenhahn and Thomas (1978); Rosner et al. (2001); Durci et al. (2002); see also wikipedia http://en.wikipedia.org/wiki/Richardson-number. The expression N for plasma with a significant contribution of radiation pressure is described in the full paper; $\omega_{sh} = dv_\varphi/dr$. In Fig. 3 the Prandtl-Karman model and the most plausible minimal value of α_t is used: $\alpha_t = 0.01$.

In the Prandtl-Karman model turbulent viscosity ν_t is calculated as

$$\nu_t = \alpha_t l_t v_t =$$

$$= \alpha_t h_\rho (h_\rho \, dv_\varphi/dr) =$$

$$= \alpha_t h_\rho^2 \, dv_\varphi/dr,$$

see equation (4.8) in the full paper. Here α_t is a non-dimensional coefficient, l_t and v_t - are respectively characteristic spatial scale (average size of vortices) and an amplitude of velocity fluctuations. Value $h_\rho(r) = [\,|d\ln(\rho)/dr|\,]^{-1}$ - is a spatial scale of density distribution $\rho(r)$. Kinematic viscosity ν_t allows the calculation of dynamic viscosity $\mu = \rho\nu$ and viscous stress w via the Newton friction law
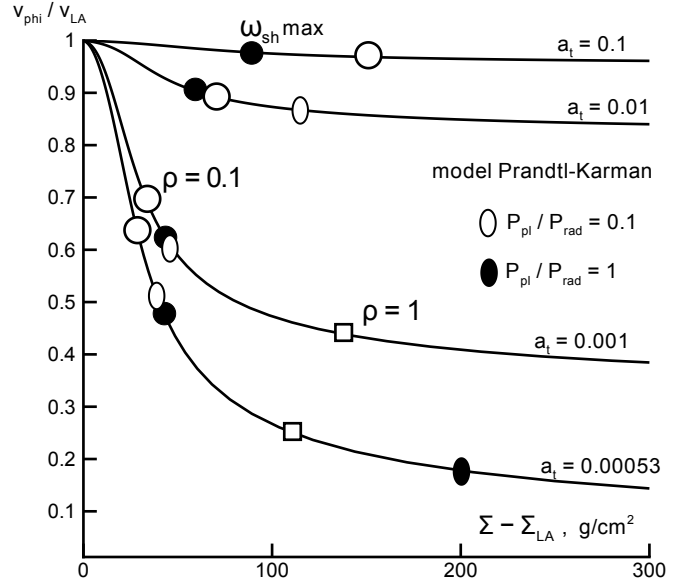
$$w = \mu \frac{dv_\varphi}{dr}.$$

FIG. 4: Decrease of linear angular velocity v_φ and sharp accumulation of column mass Σ in the process of braking of velocity. The part of the zone A, where the velocity shear is dominated, is shown. This is marked by the thick curve in Fig. 3. The filled circles indicate the maxima of the shear frequency ω_{sh}; the open circles and squares represent respectively the depths where densities are: $\rho = 0.1$ and $1 \ \mathrm{g \ cm^{-3}}$. The elliptical symbols show the ratio of plasma and radiation pressures.

The stress between the rotating fast layers and the deeper interiors of NS decreases rotation frequency with depth.

The Prandtl-Karman model is traditionally used in analyzing shear turbulence. The coefficient α_t in this model is related to the Karman constant κ (Schlichting 1965) by the formula $\alpha_t = \kappa^2$. In the case of turbulence near a wall in a medium with neutral stratification, we have

$$\kappa \approx 0.4, \quad \alpha_t \approx 0.16.$$

In the Shakura and Sunyaev (1973) model of α-friction the turbulent viscosity is

$$\nu_t = \alpha_t l_t v_t = \alpha_t h_\rho c_T.$$

Again l_t and v_t are the shear turbulence length and velocity scales, and α_t is a numerical coefficient. The vertical size of the vortices is determined by the stratification scale. We can use both the scale h_ρ (density stratification) and the scale

$$h_{ppl} = [\,|d\ln(p_{pl})/dr|\,]^{-1}$$

(thermal plasma pressure p_{pl} stratification). Since the change in temperature is small when varying the radius, these definitions are approximately equivalent. In cases, when radiatin pressure dominates, the scale h_p calculated from the total pressure can be considerably larger.
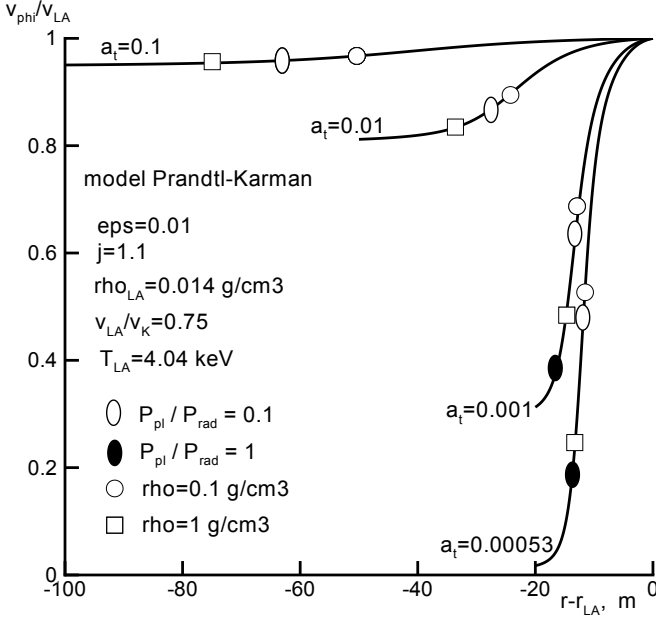
FIG. 5: Velocity profiles in the Prandtl-Karman model of friction (4.8). The influence of the coefficient α_t (the numbers near the curves) on the flow braking in the layer A is shown. The Prandtl-Karman model is traditionally used in calculations of stress in the turbulent shear flow.
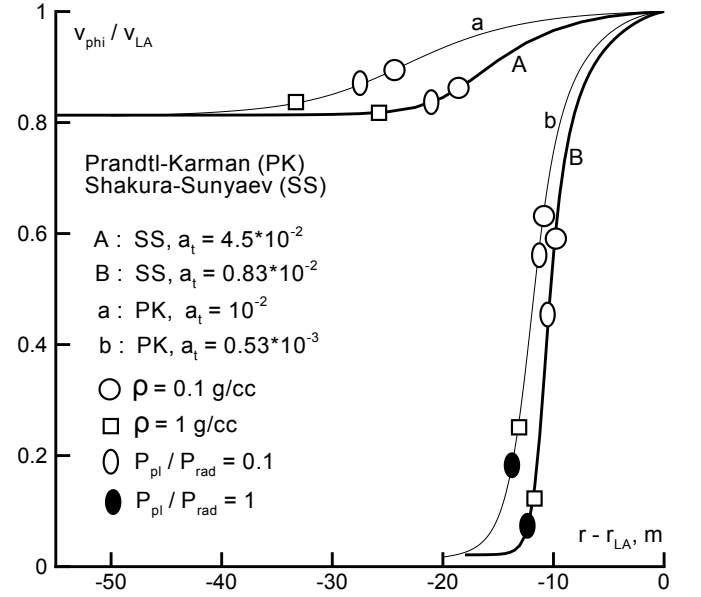

FIG. 6: Surprising universality of the conclusion about the impossibility of stopping a Keplerian flow by shear friction at a physically justified friction coefficients independent of the specific formula for the turbulent shear viscosity ν_t. Profiles a, b and A, B refer respectively to the calculations based on the qualitatively different equations (4.8) and (4.9) for viscosity ν_t. Equations (4.8) and (4.9) correspond to the Prandtl-Karman (PK) model and to the Shakura-Sunyaev (1973) α-parameter model.

Our objective is to estimate the maximum possible decrease in rotation velocity $(\Delta v_\varphi)_A$ on the layer A. This is the layer in Fig. 3 between the horizon LA and the horizon of the jump J. Such an estimation requires the minimal, physically justified viscosity ν_t. Therefore, first, we use the length h_ρ rather than h_p and, second, we use the smallest pulsation velocities v_t. Let us discuss the choice of the characteristic velocity v_t in the Shakura-Sunyaev model. The flow rotational velocity is great, $v_\varphi \sim v_K \approx 0.4\,c \approx 10^{10}$ cm s^{-1}. The adiabatic speed of sound $c_S = (0.1-0.2)v_\varphi \sim 10^9$ cm s^{-1} in the radiation-dominated medium under study is also fairly high (IS99). The subscripts S and T refer to the adiabatic and isothermal speeds of sound.

In ordinary turbulent flows at great Reynolds numbers, the velocity of turbulent pulsations is several percent of the mean flow velocity (e.g., 5-10%), then $v_t \sim 0.07v_\varphi \sim 7 \times 10^8$ cm s^{-1}. The isothermal plasma speed of sound $c_T \sim 10^8$ cm s^{-1} under our conditions is $\sim 1\%$ of the flow velocity. Ion thermal velocities are of the order of c_T. As one can see, this is the lowest velocity. Thus, the smallest scales l_t and v_t are used in the approximation of viscosity ν_t.

From what was said about the turbulent pulsation velocities $\sim 7 \times 10^8$ cm s^{-1} it follows that the coefficient α_t in the Shakura-Sunyaev viscosity should be ~ 1. But as we see from Fig. 6 much smaller coefficients are necessary to stop fast rotation in the velocity shear layer.

Under standard assumptions about the parameters of turbulent viscosity, it can reduce only slightly the velocity of the very rapid nearly Keplerian rotation of the flow that slowly settles onto the NS (see Section 8 in the full paper). We arrive at a paradoxical result: *the universally accepted parameters of turbulent viscosity give rise to a massive rotating equatorial layer in which the rotation decays very slowly and the energy release takes place mainly at depths where the matter density exceeds considerably* 10^4 *g cm*$^{-3}$.

Slow decay of the rotation velocity causes the radial component of the centrifugal force to decrease. For the same reason, the radiation flux produced through energy release due to the decay of the rotation velocity in the layers below that under consideration also decreases with depth. Both these factors cause a rapid increase in "effective" gravity with depth and a sharp decrease in pressure scale height. It is important to note that a slight imbalance between the three forces under consideration (gravity, centrifugal force, and light pressure) is enough for the local pressure scale height $h_E = 2T/m_p g_{eff}$ to begin to decrease rapidly with depth and for the matter density and its contribution to the total plasma and radiation pressure to begin to grow sharply (for a detailed analysis, see Sections 1.3 and 8).

The gravity wave ladder. The "sole" or base extends to many heights such as h_E, i.e., the density in it increases by many orders of magnitude. The difference
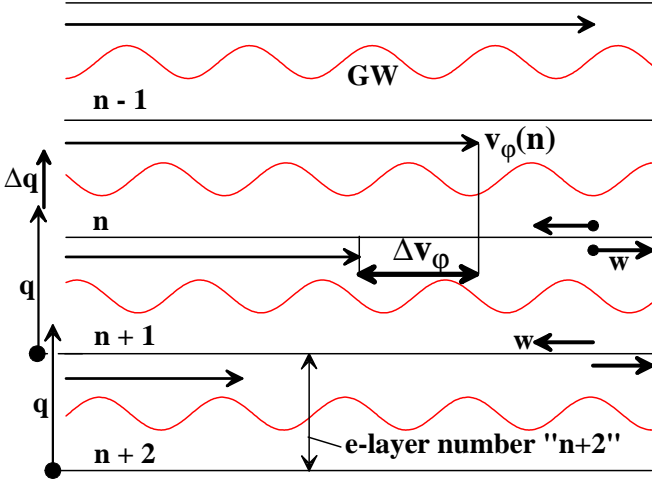
FIG. 7: Sequence or ladder of nonlinear gravity waves, each traveling in its layer with a thickness of $h_E = 2T/m_p g$ of an exponential atmosphere. The pairs of arrows w indicate the transferred shear stress through which the angular momentum is eventually transported to the bulk of the NS. The arrows $v_\varphi(n)$ indicate the average rotation velocity at the level of layer n. The arrows q and $q + \Delta q$ represent the radiation flux at the entrance to or exit from the e-layer (an increase in ρ by a factor of "e" takes place in the "e-layer"). The increment $\Delta q = w \Delta v_\varphi$ is related to wave breaking and the dissipation of kinetic energy of the gravity wave in this layer. The temperature T drops by ΔT when shifting upward by one layer to provide the removal of flux q through radiative heat conduction.

between the velocities of the azimuthal flow above and below a layer with a thickness of the order of h_E should lead to the generation of internal gravity waves propagating inside the layer under consideration in the direction of the flow. The wind above the ocean surface on Earth generates the universally known waves in exactly the same way. Nonlinear processes (wave braking) dynamically couple the waves and shear flows (differential rotation) in neighboring layers with a thickness of h_E. This makes it possible to transport angular momentum to deep NS regions through a stably stratified atmosphere made up of a "stack" or "ladder" of layers h_E (see Fig. 7).

We constructed the gravity wave ladder by assuming that a small, compared to the Keplerian velocity, but noticeable decrease in rotation velocity (a decrease by a value of the order of the local speed of sound) occurs in each layer with a thickness equal to the pressure scale height h_E (see Fig. 7). Unfortunately, full flow braking at the commonly assumed Richardson number (see Sections 1.3 and 10) Ri = 0.25 requires a large number of ladder "steps" (here, a layer of thickness h_E is called the ladder step). Increasing the shear frequency dv_φ/dr by reducing the critical value of Ri from 0.25 to 0.1 does not save the situation in the sense of an overly high mass drawn into rapid rotation (see Fig. 3), al-

though, of course, increasing the frequency dv_φ/dr allows the rotation velocity to be reduced with depth more rapidly. This approach leads to a picture with great energy release at depths corresponding to densities $\rho > 10^4$ g cm^{-3} and a mass Σ in a unit column greater than 10^7 g cm^{-2} (see Fig. 3 and a detailed discussion in Section 1).

At depths with a surface density $\Sigma > 10^9$ g cm^{-2}, the matter density rises to an extent that the Fermi energy of electrons begins to exceed the plasma temperature and the electrons in the plasma become degenerate. The density below this layer (that is in the "ocean" of degenerate electrons and thermal ions) ceases to grow exponentially with depth, the entropy ceases to decrease, and conditions for full braking of the azimuthal rotation are created. Here, we are dealing with a picture with a thick, rapidly rotating base. The presence of a lower ocean-solid crust boundary again makes the problem similar to the problem of flow braking near a wall accompanied by the formation of a logarithmic PrandtlKarman velocity profile (which was considered in detail for the problem of a levitating layer in IS99). The solid crust rotates with the NS rotation frequency.

Main equations

We use equation of mass conservation

$$\rho v_r = -\dot{\Sigma}$$

and radial force balance

$$\frac{d}{dr}(p + \rho v_r^2) = -\rho \left(g_{grav} - \frac{v_\varphi^2}{R} \right) = -\rho g_{eff}$$

to describe braking, cooling, and settling of accreting matter. Here

$$\dot{\Sigma} \sim \Sigma_T \, c/R,$$

is accretion rate per unit of NS surface, $\Sigma_T = m_p/\sigma_T$, σ_T is Thomson cross-section, R is radius of neutron star, v_φ and v_r are rotational and radial components of velocity. The last corresponds to settling of matter.

Equation of state is

$$p = p_{pl} + p_{rad}, \quad p_{pl} = \rho \frac{2T}{m_p}, \quad p_{rad} = \frac{aT^4}{3},$$

where p_{pl} and p_{rad} are plasma and radiative pressures.

Conservation of angular momentum gives

$$w = J - \dot{\Sigma} \, v_\varphi.$$

This conservation law follows from equation

$$\frac{\partial(\rho \, v_\varphi)}{\partial t} = -\frac{\partial(\rho \, v_\varphi \, v_r)}{\partial r} + \frac{\partial w}{\partial r}$$

in the steady-state case when $\partial_t = 0$. The constant

$$J \sim \dot{\Sigma} v_K$$

is an integral of this equation; here v_K is Keplerian velocity.

Newton friction law for turbulent viscous stress is

$$w = \rho\, \nu\, dv_\varphi/dr,$$

where ν is total kinematic viscosity

$$\nu = \nu_i + \nu_{rad} + \nu_t.$$

Partial viscosities are

$$\nu_{rad} = \frac{4}{15} \frac{a\, T^4 \Sigma_T}{c\, \rho^2} \simeq \frac{\rho_{rad}}{\rho}\, l_T\, c$$

(Weinberg, 1972), here $\rho_{rad} = aT^4/c^2$ is "density" of photons, $l_T = 1/n\sigma_T$ is photon mean free path and $n = \rho/m_p$. Ion viscosity is

$$\nu_i = 10^3\, \frac{T^{2.5}}{\rho\, \ln\Lambda},$$

where Λ is Coulomb logarithm (Spitzer, 1962), temperature is in keV, while density and kinematic viscosity are in g/cc and $\mathrm{cm^2/\,s}$. Under the physical conditions in the spreading layer the radiative viscosity often exceeds the ionic one, but the turbulent viscosity dominates.

Turbulent viscosities ν_t in case of shear flow with weak stratification has been given above.

In the case of insignificant gravity stratification the braking of rotation as result of viscous deceleration is

$$\frac{dv_\varphi}{dr} = \frac{1}{\rho} \frac{w}{\nu} = \frac{1}{\rho} \frac{J - \dot{\Sigma} v_\varphi}{\nu_i + \nu_{rad} + \nu_t}.$$

In the alternative case of significant gravity stratification we use another description of the deceleration of rotation (decrease in shear frequency v'_φ). This another description is

$$\frac{dv_\varphi}{dr} = \frac{N}{\sqrt{\mathrm{Ri}}}.$$

Here N is the Brunt-Väisälä frequency and Ri is Richardson number. This frequency in the case of large contribution of radiation pressure p_{rad} in the layer transmitting radiative energy flux q is

$$N^2 = g_{eff}^2(c_T^{-2} - c_S^{-2})\left(1 - \frac{1}{2}\,\tilde{q}\, \frac{10 + 8\tilde{R} + 5/(4\tilde{R})}{1 + 4\tilde{R}}\right),$$

(see Appendix in the full paper). Here ratio $\tilde{R}$ and normalized flux $\tilde{q}$ are

$$\tilde{R} = \frac{p_{rad}}{p_{pl}}, \quad \tilde{q} = \frac{q}{g_{eff} c \Sigma_T}.$$

The deceleration v'_φ changes from $v'_\varphi = w/\rho\nu$ (if $0 < \mathrm{Ri} < 0.25$) to $v'_\varphi = N/\sqrt{\mathrm{Ri}}$ (if $\mathrm{Ri} \approx 0.25$) depending on local value of the number Ri.

Energy balance

$$-\dot{\Sigma}\left(\frac{v_r^2 + v_\varphi^2}{2} + 5\frac{T}{m_p} + \frac{4}{3}\frac{a T^4}{\rho} + \psi\right) - w v_\varphi + q = Q$$

presents advection of rotational and radiation energies $\dot{\Sigma}(v_\varphi^2/2 + 4\, a\, T^4/3\rho)$, viscous dissipation $w v_\varphi$, and radiative flux

$$q = -\frac{c\, \Sigma_T}{3\rho} \frac{d(a\, T^4)}{dr}.$$

They are the main contributions to the energy balance. The terms connected with advection of kinetic energy of radial motion $v_r^2/2$, thermal energy of plasma T/m_p, and gravitational energy ψ are small (nevertheless all they are included into solution). Changes in gravitational energy appears due to motion of matter in radial direction. Radial shifts are small therefore the term ψ is negligible. Value Q is the constant (integral) of integration. It is defined by boundary condition at large depth. Value of Q is connected with energy flux coming from the large depth. This value is small in comparison with the main terms listed above.

The Existence of X-ray Bursters Argues against a Massive Base

Weak braking leads to slow decay of the azimuthal velocity as one recedes from the levitating layer downward along the radius. Therefore, significant heat release at great depths is associated with it. Note that the store of energy in a nearly Keplerian azimuthal motion exceeds the energy being released not only in pycnonuclear reactions but also even during the burning of accreting hydrogen to produce helium by more than an order of magnitude. Figure 8 shows that slow braking (without any abrupt decrease in velocity v_φ) leads to a high temperature (up to 150 keV) at great depths. The temperature rises inward to provide the outward removal of the energy being released, i.e., to produce a temperature gradient capable of maintaining the corresponding radiative energy flux (see Figs. 3, 8, and 9). This energy release is much greater than the heating through contraction as the accreting layer corotating with the star settles down.

According to the simplest one-dimensional models (disregarding the presence of a spreading layer), at a high rate of spherically symmetric accretion, the temperature in a zone with a surface density $\Sigma \sim 10^9$ g cm^{-2} turns out to be so significant that helium in it burns stationarily rather than explosively, i.e., without giving rise to X-ray bursts (for a review, see, e.g., Strohmayer and Bildsten 2006). Disk accretion and the presence of a spreading layer with a thick base should also lead to a dramatic
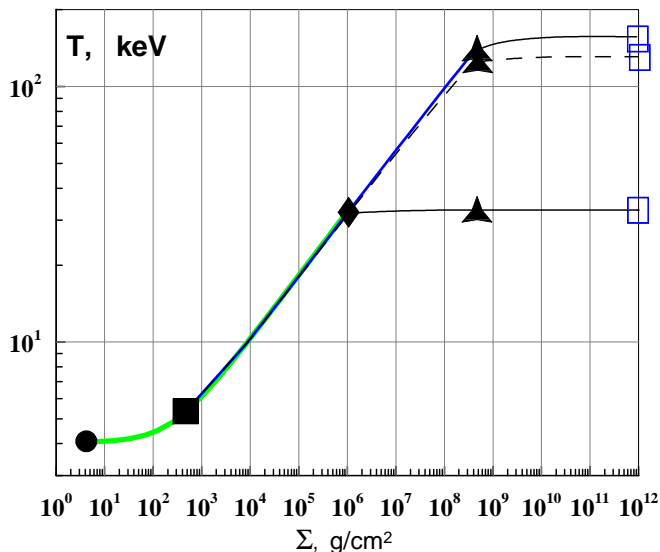
FIG. 8: Rise in temperature T deep into the base in our calculations with the Richardson number Ri =0.25 (upper curve), with Ri =0.1 (middle curve), and for the case with a velocity jump J (see Fig. 3; in Fig. 3 the jump J lies between the diamonds) (lower curve). In the first two cases, the rotation decays at large depths (see Fig. 3) with a great optical depth. This causes a dramatic rise in temperature on the horizon of nuclear helium flashes marked by the triangle. The transition from the exponential atmosphere to the ocean of degenerate fluid is located approximately on the same horizon. The diamond corresponds to jump J; the change in friction mechanism from turbulent viscosity to a gravity wave ladder is marked by the filled square; the open square indicates the location of the upper boundary of the solid NS crust.

FIG. 9: Profiles of the radiation flux q for the cases with a jump in velocity v_φ and with a gravity wave ladder. In the presence of jump J, the flux q terminates immediately under the jump due to a dramatic slowdown of the rotation velocity v_φ. The flux q is produced by the dissipation of rotational kinetic energy. The markers denote the following: circle 1 – the boundary LA of levitation on the verge of a wind (the layer L is to the right of point 1); 2 – the change in friction regime; 3 – the horizon on which jump J can be located; 4 – the horizon under the jump; 5 – the atmosphere-ocean boundary; 7 – the crust (the crust position is different for different profiles, because it is measured from boundary LA); 6 – the position of the atmosphere-ocean horizon in the case of a gravity wave ladder without any jump J. The profile 1-2-3-4-5-7 contains a jump. There are the segment of turbulent friction 1-2, the ladder 2-6 with Ri =0.25, and the second segment of turbulent friction in the ocean 6-7 on the profile 1-2-3-6-7. The profile on which v_φ is nulled at a depth of 600 m was constructed by assuming the absence of an ocean when the exponential atmosphere extends to the depth of 600 m. The distribution $q(r)$ and the optical depth define the distributions of the radiation energy density and temperature in Fig. 8.

temperature rise in the helium burning zone and to the switch-off of X-ray bursts (see Fig. 8). Moreover, the mechanism with a long "ladder" and a great spun-up mass leads to a temperature rise on the flash nucleation horizon even at moderate accretion rates, when the stationary luminosity of the X-ray source is $\sim 10\%$ of L_{Edd}. Most of the bursters are active precisely at these persistent luminosities of the source.

Quasi-periodic oscillations of the radiation flux with a frequency close to the NS rotation frequency are observed during intense bursts (Strohmayer and Bildsten 2006). This is direct evidence that the base rotating with a high frequency in these sources does not reach the helium burning zone. In this case, the burning zone rotates with a frequency close to the rotation frequency of the central NS regions.

There is no doubt that the mechanism for the operation of X-ray burst sources is fairly complex – most bursters are known to exhibit bursts by no means constantly. Series of bursts or single bursts are observed from many of them very rarely and occasionally recur only tens of years later (see, e.g., Linares et al. (2010) for the source Circinus X-1). It is quite possible that in
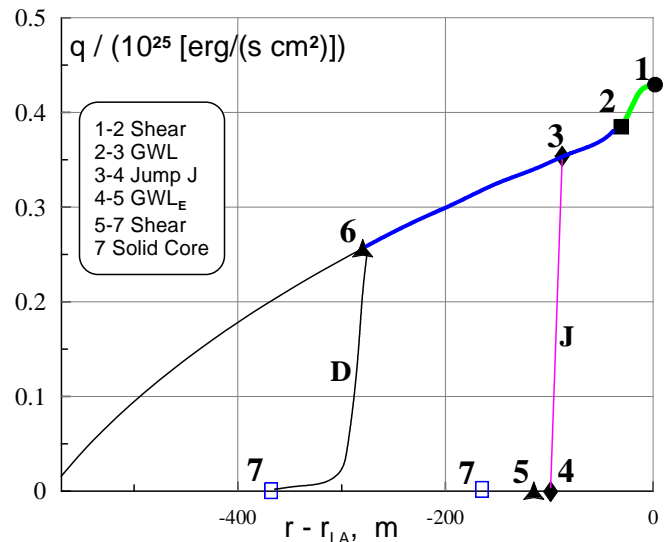
some of these sources we are dealing with a thick base with a high temperature in the helium burning zone, because of which no bursts are usually observed in them. In a layer with $\rho \sim 10^5 - 10^6$ g cm^{-3}, a temperature of ~ 50 keV is enough for stationary helium burning to take place without any nuclear explosions that lead to the observed phenomenon of X-ray bursters. However, when a burster begins to manifest itself, we must recognize that nature finds ways to brake the rotation of the accreting matter in a layer located well above the zone of explosive helium burning.

Giant Solitary Gravity Wave As a Way to Stop the Rotation in the Base

The analysis performed below in Section 1 leads to a picture with a giant solitary gravity wave (GSGW) at a depth that corresponds to a surface density of $10^5 - 10^6$ g cm^{-2}. Such a wave can have the shape of a solitary structure on the equatorial perimeter $[0, 2\pi]$, which is shown in Fig. 10, or can be a set of several non-equidistant crests on the perimeter. In this case, there are crest fluctuations. Because of the latter, when averaged over the azimuthal angle φ from 0 to 2π, the amplitude of the first azimuthal Fourier harmonic is nonzero. Such a nonlinear wave brakes the rotation of the matter that falls from the levitating layer L. The ratio of the wave amplitude to the pressure scale height h_E and not to the wavelength is a measure of nonlinearity. The GSGW efficiently interacts both with the rapidly rotating gas in the overlying layer and with the underlying layer that rotates considerably more slowly than it. Owing to this hydrodynamic interaction, the force accelerating the rotation of the NS as a whole is transferred downward to the solid crust. These issues are discussed in detail in Sections 1.3 - 1.6.

Such a long-lived feature in the flow can emerge in a rapidly rotating atmosphere, just as long waves are generated by a continuous wind during floods in St. Petersburg. It is important that this hypothesis can remove the difficulty noted above in the theory of X-ray bursters by greatly reducing the stationary temperature in the helium burning layer (see Fig. 8) and opening the possibility of explosive helium burning. At present, this hypothesis seems a more reasonable solution than the assumption about anomalously low values of the viscosity coefficients (hundreds of times lower than those observed in the Earths atmosphere and ocean and in large-scale laboratory experiments) or about a sharp decrease (few times) in Richardson coefficient when the ladder of interacting gravity waves is considered in a bursters exponential atmosphere. With this publication, we hope to draw the attention of specialists in wave dynamics to this very interesting and as yet incompletely solved problem.

The explosive helium burning ignition zone is located on the equator. In the picture with a GSGW, the temperature under it turns out to be considerably higher than that in the commonly considered example of the accretion of matter without any angular momentum onto a neutron star (Strohmayer and Bildsten 2006). Consider the case of a thin base with a GSGW. Let us single out two horizons: the horizon on which the GSGW is located ($\rho \sim 10^3$ g cm^{-3}, $\Sigma \sim 10^6$ g cm^{-2}) and the helium flash horizon ED between the exponential atmosphere E and ocean D (see Fig. 11). At the level ED, we have $\rho \sim 10^6$ g cm^{-3} and $\Sigma \sim 10^9$ g cm^{-2}.

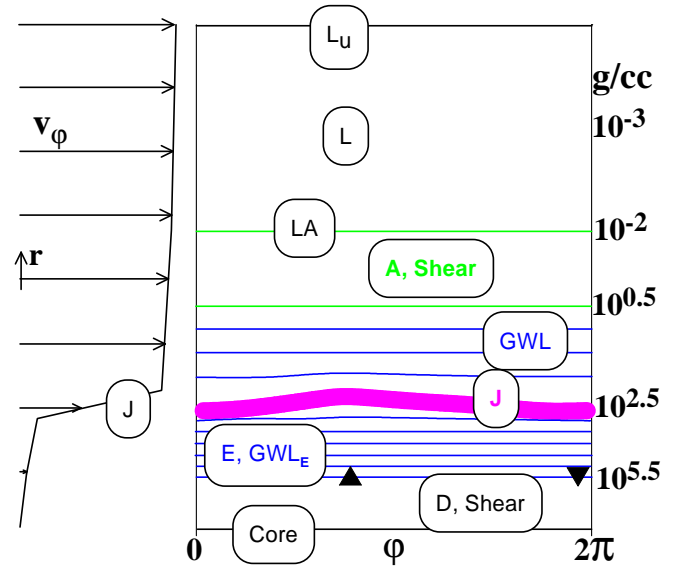The temperature rise under the GSGW is related to rapid dissipation of the azimuthal velocity and great en-

FIG. 10: Velocity jump J and giant solitary gravity wave (GSGW) on the period $[0, 2\pi]$ of the equatorial perimeter φ. The extent of the perimeter is 60 km. The velocity and density [g cm^{-3}] profiles in the corresponding layers are shown on the left and the right, respectively. The designations of the layers and boundaries between them are listed below on the scheme of the vertical structure in Fig. 13. The gravity wave ladders are schematically shown in the form of a sequence of e-layers, as in Fig. 7. The drop in velocity v_φ occurs at the broadened GSGW boundary shown in the form of a wide stripe. The main heating of photons takes place in this stripe smoothed by mixing of gases by oblique shock waves. The horizontal and vertical scales differ greatly – the GSGW steepness is less than 10^{-3}. The triangles at level ED (at which a thermonuclear flash ignites) mark the GSGW maximum and minimum along the φ-axis. They are important for the explanations that associate the rise in pressure under the GSGW with the initiation of a helium flash at a point on the NS surface (see Section 1.8).

ergy release near the GSGW, where the velocity jump is located (see Figs. 3 and 9). The temperature constancy downward along the radius (in the zone where there are no energy sources) is the result of energy conservation during the transport of radiation in the radial column without any lateral losses. Such a temperature profile is established in a time much longer than the diffusion time of the radiation from the layer under consideration.

The GSGW is located at equatorial latitudes, where the velocity v_φ (in the levitating belt and the base under it) is at a maximum. Strong energy release in the equatorial zone in the simplest approximation of a radial column without any lateral losses should lead to a high temperature in the explosive helium burning zone. A high temperature makes this zone favorable for the ignition of nuclear reactions of rapid helium burning.

Let us try to take into account the lateral losses in the radial column of matter and their influence on the depen-
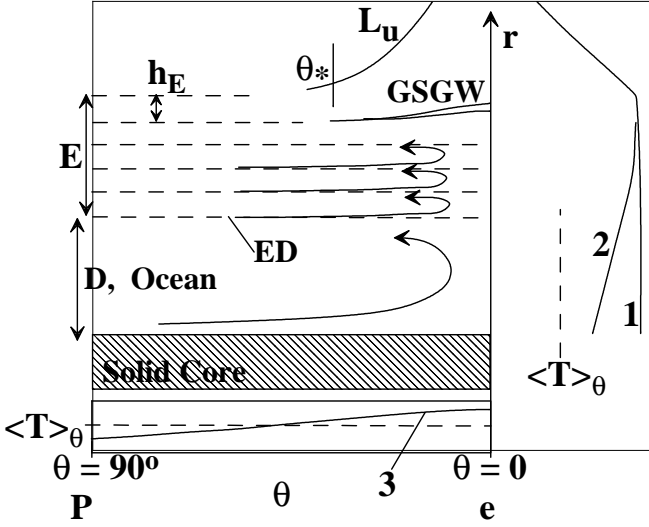
FIG. 11: Thermal matching of the zone of GSGW energy release and high-density NS envelopes. The meridional NS section and the radial temperature profile $T(r)$ on the equator (curves 1 and 2 on the right) as well as the meridional temperature profile $T_{ED}(\theta)$ (curve 3 below) are shown. Curve 1 was constructed without allowance for the lateral losses. These losses were taken into account in curve 2. The lateral energy losses from the radial column were caused by meridional convective circulation. The temperature at the level ED averaged over the meridian θ is denoted by $\langle T \rangle_\theta$. It is marked by the dashed straight lines on the right and bottom plots. The high-density envelopes include: atmosphere E, ocean D, and the solid crust. In addition, the photosphere L_u (the zone above which the optical depth is close to unity) above the levitating belt L and the boundary of the belt L in latitude $\theta_\star$ are shown; P and e are the NS pole and equator, respectively. The loops indicate convective circulation in ocean D and atmosphere E. In the atmosphere, circulation takes place in layers with a thickness equal to the pressure scale height h_E.
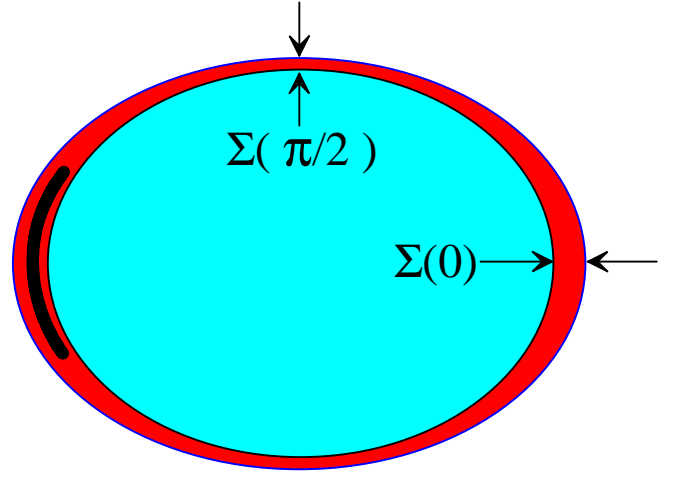

FIG. 12: The red layer is the layer of fresh accreted material (fuel) corotating together with neutron star. Fresh material is less dense than underlying ashes (blue) from previous bursts. The burst begins at the interface between red and blue. On rotating star the mass thickness $\Sigma(\theta)$ [g/cm^2] of fresh material is function of latitude θ. The Σ is thicker at equator: e.g., $\Sigma(0)/\Sigma(\pi/2) - 1 = 1.5 \cdot 10^{-2}$ for rotation frequency of star 200 Hz. Heat conduction is inversely proportional to Σ. Therefore at equal power of heat production per unit of surface, temperature is higher under thicker layer. This heat is produced by thermonuclear reactions at the stage preceding the approaching instant of beginning of burst. Therefore a thermonuclear burst starts at equator. The black curve at the left side of the red layer marks the horizon of giant solitary gravity wave (GSGW). Radial thicknesses of fresh sublayers above and below the horizon do not correspond to those shown in the sketch. Geometrically the above sublayer is thicker, see Fig. 14. Above the horizon the fresh material rotates faster. But thickness $\Delta\Sigma$ above the horizon is much less ($\sim 10^{-4}$) than Σ of whole fresh layer. The addition $\Delta\Sigma$ is insignificant for the ratio $\Sigma(0)/\Sigma(\pi/2)$.

dence of the temperature $T_{ED}(\theta)$ on the helium burning horizon ED on meridional angle θ. The result of our estimations is schematically shown in the lower inset in Fig. 11. Below the horizon of jump J and the GSGW, the matter is in corotation with the NS (envelopes E, D, and the crust in Fig. 11). Because of the very high density and, accordingly, heat capacity of the matter in the exponential atmosphere and in the ocean with degenerate electrons, the lateral losses are significant (the speed of sound depends weakly on radius, while the density rises by several orders of magnitude). The ratio of the densities on the horizons of jump J and helium flash ED is approximately three orders of magnitude. At such a density ratio, lateral cooling causes a decrease in temperature at level ED under jump J compared to the temperature immediately under the jump (≈ 30 keV, see Fig. 8). This decrease is seen on curve 2 on the right in Fig. 11 (cf. curves 1 and 2). Level ED is highlighted by the triangle in Fig. 8, while the level of jump J is marked by the

diamond in Fig. 8.

Despite the presence of lateral losses, the function $T_{ED}(\theta)$ (curve 3 in the lower inset in Fig. 11) has a maximum on the equator (because the heating source is located above it). For this reason and since the optical depth $\tau(\theta) \propto \Sigma(\theta)$ above horizon ED is at a maximum on the equator (see Fig. 12), the flash will begin on the equator (see Section 1.7). The value of τ above the flash horizon is very important in the theory of a thermal explosion when the competition between heating and cooling leads to an explosion. The heating is related to the production of heat in reactions, while the cooling is related to the radiative heat removal through the optical depth. Clearly, poor heat removal contributes to the explosion.

The burst begins in the point at the equator, see Fig. 13.

The importance of allowance for the stellar rotation and general relativity effects. Observations of the millisecond pulsar/burster SAX J1808.4-3658

$$\Delta t \sim 10^{-3} \text{ s}$$
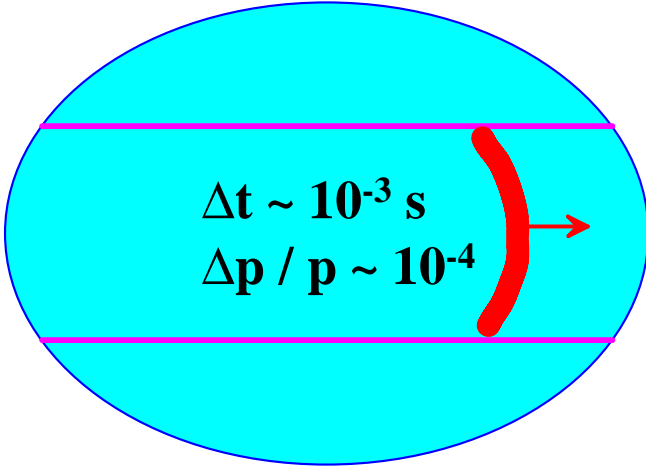$$\Delta p / p \sim 10^{-4}$$

FIG. 13: Gathering of thermonuclear fuel (fresh material) at equator (see Fig. 12) and initiation of burst at equator under the crest of giant solitary gravity wave (GSGW). The crest of GSGW is shown by the red curve. It is marked also by the triangular directed up in Fig. 10. GSGW propagates along the arrow. It propagates above the red/blue surface corresponding to the bottom of the layer of fresh material, see Figs. 10 and 12. GSGW moves under the levitating belt confined in meridional direction between the two horizontal lines. GSGW rises pressure under its crest. The rise of pressure under crest Δp, normalized to hydrostatic pressure p at the bottom of fuel, is $\Delta p/p \sim 10^{-4}$. This rise is significant since it lasts rather long $\Delta t \sim (\lambda/2)/v_{GSGW} \sim 10^{-2} - 10^{-3}$ s; here $\lambda \sim 60$ km is wavelength of GSGW and $v_{GSGW} \sim 10^{8}$ cm/s is its velocity (the red arrow) relative to matter corotating with neutron star. This significant and extended time rise of pressure and temperature ignites fuel in a point when fuel in the bottom is very near to the ignition state.

showed that this transient X-ray source in a binary system with a period of 2 h (Chakrabarty and Morgan 1998) occasionally exhibits X-ray bursts associated with nuclear explosions (in 't Zand et al. 1998), manifesting itself in a different state as an X-ray pulsar with a period of 2.49 ms (Wijnands and van der Klis 1998). During its activity, the source's luminosity changed rapidly from 6×10^{36} to 2×10^{34} erg s^{-1}, with the luminosity having been halved in a time of the order of several hours (Gilfanov et al. 1998). This example clearly demonstrates the following: (a) the mechanism of bursters does not work all the time but only under certain conditions (possibly, when a giant solitary wave appears), (b) neutron stars rotate rapidly and their rotation velocity on the surface can reach 1/5–1/4 of the Keplerian velocity, and (c) there is disk accretion onto the NS at a sufficiently high luminosity of the source – no other option is possible in such a close binary system. More than twenty neutron stars with weak magnetic fields and rapid rotation are known to date (van der Klis 2006). We consider the influence of stellar rotation on the structure of the levitating layer and its base in a different paper (Inogamov

and Sunyaev 2011). We show that the stellar rotation velocity observed in these objects does not change radically the results of IS99 and this paper, but it should be taken into account.

The dynamics of the spreading layer and its base is complex, while the physical conditions in it are very far from those in laboratory experiments and commonly considered problems related to the atmosphere and ocean as well as to the motion of aircraft and rockets and the braking of asteroids and satellites in the atmosphere. In this situation, it is natural to take the first steps by neglecting the effects of general and special relativity.

Nevertheless, allowance should be made for the fact that the luminosity of the spreading layer is twice that of an extended accretion disk even for a non-rotating NS with a radius $3R_g$, where $R_g = 2GM/c^2$ (Sunyaev and Shakura 1986). In the Newtonian problem, these two quantities are equal. The Keplerian velocity near the surface in the Schwarzschild metric is more than half the speed of light, while it is close to $0.4\,c$ in the Newtonian approach. The effects of rapid NS rotation (and counterrotation) on the luminosity of the spreading (or boundary) layer were studied in detail by Sibgatullin and Sunyaev (2000) in terms of general relativity. These effects are great.

The luminous flux, radiation-dominated plasma in the levitation belt, and photon bubbles. Here, we investigate the hydrodynamic stability of the levitating layer and the underlying base (see Section 10 and the Appendix). We show that the levitating layer is close to a neutral stability: there are neither radial convection nor gravity waves.

In atmosphere and ocean physics, a neutrally stable medium is called subtile. Convection under the dominance of radiation pressure would lead to a partial spatial separation of radiation and matter and to the formation of buoyant photon bubbles. In the base, the ratio of the radiation and thermal pressures decreases rapidly as the density rises. Nevertheless, the radiation pressure accounts for an appreciable fraction of the plasma pressure as long as the matter remains rapidly rotating one and this is despite the dramatic rise in density.

It is unlikely that it will be possible to maintain the balance of three forces (gravity, the centrifugal force, and the force associated with the radiation pressure gradient) necessary for levitation, first, at a level of a few thousandths of the weight and, second, everywhere with the sign that provides the pressing of matter to the star. In IS99, we constructed a stationary solution with the satisfaction of the condition for compensation at a level of a few thousandths along the entire base of the levitating belt from the equator to latitude $\theta_\star$ (see Fig. 1). However, analysis of the meridional equilibrium in the base (see section 1.10) leads to the conclusion that the meridional extent of the base is slightly less than that of the levitating belt $\theta_\star$. As a result, the scenario with the

hurling of matter upward along the radius (like a wind) in the equatorial zone and with the sinking of this matter back onto the NS surface at latitudes $\sim \theta_\star$ should be realized. The wind lifting height on the equator is limited, because the luminous flux diverges in radial directions in a spherical geometry. The divergence of the luminous flux is disregarded in the IS99 solution, which is constructed in the approximation of a thin layer on the NS surface without allowance for the curvature of the NS surface.

Such a flux outgoing on the equator and returning at latitudes $\sim \theta_\star$, first, enhances the advection of radiation (see Fig. 2) and, second, makes this circulation random. According to the IS99 calculations, the meridional rotation period of such a large-scale random circulation loop is of the order of the rotation period of a matter particle in the levitating belt around the NS. Accordingly, the instantaneous luminosity of the levitating belt as a function of the azimuthal angle φ contains a significant contribution from the first Fourier harmonic in φ. This can explain the appearance of the upper peak in the kilohertz variability of radiation from the boundary layer (see also Sections 1.8 and 1.11 below). Since the radiation circulation is random in nature, the Q factor of the peak turns out to be small. The question of why the lower peak appears is considered in Section 1.11.

Meridional force balance in the case of a thick base. Consider the hydrostatic balancing of matter in the radial and meridional directions for a thick, rapidly rotating base. Rapid gas rotation in the case of a thick, massive base gives rise to a significant force of centrifugal rolling toward the equator. We compare two cases: (1) with a thick base and without any jump at the GSGW that reduces sharply the rotation velocity and (2) with a thin (in radius and mass) base in which there is a jump in velocity v_φ (see Figs. 3 and 9 and the text below; in Figs. 3 and 9, the jump is denoted by the letter J). Figures 9 and 3, 8, respectively, illustrate that the thick base is several times thicker in radius and several orders of magnitude thicker in surface density Σ.

It follows from Fig. 9 that, in the first case (thick base), the thickness of the layer of rapid (compared to the NS rotation frequency) rotation is about 300 m. In the second case, this thickness is 100 m. The profiles in Figs. 3, 8, and 9 were obtained by integrating the equations derived in Sections 3–7. In particular, the equations include the production of radiation energy, the outward radiation transport, and the dynamical contribution of the light pressure. A base thickness of ~ 300 m means that an equatorial swelling about 300 m in height in the form of a belt rotating relative to the NS appears on the NS surface S (see Fig. 14).

The velocity components other than the rotation velocity (radial settling and meridional spreading) are low and, hence, dynamically insignificant. When the centrifugal force is taken into account, the swelling is then
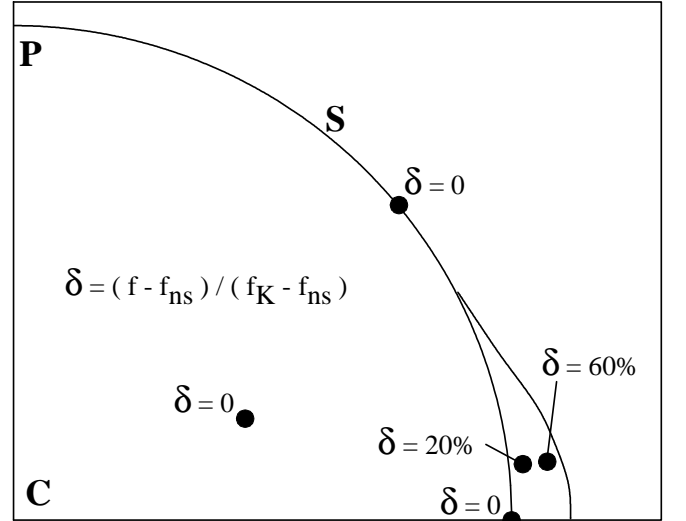

FIG. 14: Formation of a very massive swelling on the NS surface S due to nearly Keplerian rotation under the levitating layer L in the case of a spreading layer with a thick base. In the swelling zone, the matter rotates differentially and is supported by centrifugal forces.

in hydrostatic equilibrium. The meridional scale of the swelling exceeds its radial extent. Accordingly, for the description in the first approximation, it is admissible to use one-dimensional balances along the vertical, as is done in Sections 3–6. The swelling in Fig. 14 is associated with high-density matter. This qualitatively distinguishes it from the low-density levitating belt L in Fig. 1 with a density $\rho_L \sim 10^{-3}$ g cm^{-3}. As we see, not only the physical conditions on the horizon of helium flashes (the high-density horizon, see below) but also the geometry of the zone with differential rotation change significantly in the case with a thick base. The changes in geometry give rise to an equatorial swelling. Only high-density ($> 10^4$ g cm^{-3}) regions were attributed to this zone.

The radiative-meridional equilibrium in the second case (where there is a jump in velocity v_φ, a thin base) is discussed in Section 1.10. In this case, there is a slight rise of surface LA "balancing on the verge of a wind" above the NS surface. Surface LA separates the levitating matter and the base.

The Flow Structure: The Keplerian Flow–Star Interaction Mechanics

We investigate the spreading layer that emerges in the region of contact between the accretion disk and the surface of a nonmagnetic NS. The spreading layer consists of the upper rapidly rotating and lower slowly rotating parts. The rotation frequency is of the order of the Keplerian one in the upper part and is approximately equal to the stellar rotation frequency in the lower part. This

layer is shown to be a complex three-dimensional structure in the meridional (θ), radial (r), and azimuthal (φ) directions. In the first approximation, the spreading layer is axisymmetric – it forms an equatorial belt with azimuthal rotation, meridional spreading, and radial accretion settling. In the next approximation, it is natural to consider the large-scale azimuthal inhomogeneity. It is most likely this inhomogeneity that is responsible, first, for the observed quasi-periodic oscillations at a frequency of the order of one kilohertz and, second, for the splitting of these oscillations into two peaks – upper and lower (see, e.g., van der Klis 2006). The peaks shift in position within a fairly wide range, depending on the accretion rate $\dot{M}$, with the frequency difference equal to the NS rotation frequency retaining its value. The shifts of the peaks are consistent with the views of a levitating belt whose width depends on $\dot{M}$. In this case, the lower peak is produced by the collisions of the inhomogeneity in the levitating belt with the disturbance associated with the GSGW under the base (see Section 1.11 below).

The upper part of the spreading layer is broken up into two layers by surface LA. The upper layer above this surface is extended along the radius through levitation (L) in the field of gravity. It was called the levitating belt in IS99. This is a radiation-dominated layer in which levitation is achieved through an almost complete radiation compensation for the sum of the gravitational and centrifugal accelerations (the Eddington radiation support in the gravitational field). Therefore, surface LA may be called the boundary at which the balancing of matter on the verge of a wind begins. Under this boundary, the radiation flux q is slightly less than its critical (i.e., local Eddington) value. Accordingly, as one recedes from LA downward, there is a rapid rise in density with depth called in the paper condensation or accumulation (A, hence the designation LA). Along the radius, the accumulation layer A is much thinner than the levitating belt L.

The accretion flow falls into the belt L through the neck that separates the disk and the spreading layer. Above the neck, the angular momentum is transported over the disk to infinity by α-friction. The angular momentum $\approx \dot{M} v_K R$ brought by the flow into the spreading layer is transported downward to the star; here, v_K and r are the Keplerian velocity and the stellar radius, respectively. This angular momentum gives rise to a torque acting on the star. We analyze a complex system of gravity waves traveling in dense underlying layers. They are excited dynamically under the action of tangential stress w that is produced during the distribution of torque per unit surface area of contact between the belt L and the star. The existence of gravity waves is related to a sharp rise in density ρ and to stratification stability. In turn, the rise in ρ and the stability are attributable to an extreme radiative heat transfer efficiency in the optically thick case where the temperature of the spreading layer

and high-density stellar envelopes is much lower than the virial temperature under any heat releases up to the Eddington limit.

Observational Manifestations of the Spreading Layer

The IS99 model of a levitating layer with bright bands of X-ray emission had a number of clear observational predictions. The radiation from this layer should be highly variable on much shorter time scales than those for the radiation from an extended accretion disk (for a discussion, see also Sunyaev and Revnivtsev 2000).

The bulk of the energy release in the spreading layer takes place at a great optical depth in its base. As a result, the base forms a blackbody spectrum that subsequently passes through a hotter levitating plasma flow with a finite optical depth for Thomson scattering and a negligible optical depth for bremsstrahlung processes. Saturated Comptonization of photons from the base forms the observed radiation spectrum in the hotter levitating layer similar to a diluted blackbody spectrum (Sunyaev and Titarchuk 1980). Detailed calculations of the radiation spectrum forming in the spreading layer were performed by Grebenev and Sunyaev (2002) and Suleimanov and Poutanen (2006). Gilfanov et al. (2003) and Revnivtsev and Gilfanov (2006) suggested and successfully implemented a method for extracting the radiation spectrum of the boundary layer based on an analysis of the rapidly varying radiation component in X-ray sources. Savolainen et al. (2009) and several other observational groups are conducting a systematic search for manifestations of the boundary layer on the surface of accreting neutron stars using INTEGRAL and RXTE data. A detailed theoretical study of the physical processes in the base of the spreading layer must lead to new specific observational predictions.

Below, we make an attempt to solve the formulated problem. The picture of the flow as a whole is described in Section 1. The results regarding the rapidly rotating low-density levitating belt L are summarized in Section 2. The dynamical and thermal equations are derived in Sections 3–7. Section 8 is devoted to the crisis of friction with turbulent viscosity. Finally, in Sections 9–11, we analyze the influence of radiative viscosity (Section 9), the generation of buoyancy-related gravity waves (Section 10), and supersonic effects (Section 11).

REFERENCES

1. N. Babkovskaya, A. Brandenburg, and J. Poutanen, Mon. Not. R. Astron. Soc. **386,** 1038 (2008).

2. D. Chakrabarty and E. Morgan, Nature **394,** 346

(1998).

3. R.L. Cooper and R. Narayan, Astrophys. J. **657,** L29 (2007).

4. L.J. Dursi, A.C. Calder, A. Alexakis, et al., arXiv:astro-ph/0207595 (2002).

5. D.K. Galloway, M.P. Muno, J.M. Hartman, et al., Astrophys. J. Suppl. Ser. **179,** 360 (2008).

6. M. Gilfanov, M. Revnivtsev, R. Sunyaev, and E. Churazov, Astron. Astrophys. **338,** L83 (1998).

7. M. Gilfanov, M. Revnivtsev, and S. Molkov, Astron. Astrophys. **410,** 217 (2003).

8. S.A. Grebenev and R.A. Sunyaev, Astron. Lett. **28,** 150 (2002).

9. N.A. Inogamov and R.A. Sunyaev, Pisma Astron. Zh. **25,** 323 (1999) [Astron. Lett. **25,** 269 (1999)].

10. N.A. Inogamov and R.A. Sunyaev, Pisma Astron. Zh. (2011) (in press).

11. R. Kippenhahn and H.-C. Thomas, Astron. Astrophys. **63,** 265 (1978).

12. M. van der Klis, in Compact Stellar X-ray Sources, Ed. by W.H.G. Lewin and M. van der Klis (Cambridge Univ., Cambridge, 2006), p. 39; arXiv:astro-ph/0410551.

13. K.R. Lang, Astrophysical Formulae (Springer, Berlin, Heidelberg, New York, 1974).

14. W.H.G. Lewin, J. van Paradijs, and R.E. Taam, Space Sci. Rev. **62,** 223 (1993).

15. M. Linares, A. Watts, D. Altamirano, et al., Astrophys.J. Lett. **719,** L84 (2010).

16. F. Peng, E.F. Brown, and J.W. Truran, Astrophys. J. **654,** 1022 (2007).

17. R. Popham and R.A. Sunyaev, Astrophys. J. **547,** 355 (2001).

18. M.G. Revnivtsev and M.R. Gilfanov, Astron. Astrophys. **453,** 253 (2006).

19. R. Rosner, A. Alexakis, Y.-N. Young, et al., arXiv:astro-ph/0110684 (2001).

20. P. Savolainen, D.C. Hannikainen, O. Vilhu, et al., Mon. Not. R. Astron. Soc. **393,** 569 (2009).

21. H. Schlichting, Grenzschicht-Theorie (G. Braun, Karlsruhe, 1965) [in German].

22. N.I. Shakura and R.A. Sunyaev, Astron. Astrophys. **24,** 337 (1973).

23. N.R. Sibgatullin and R.A. Sunyaev, Astron. Lett. **26,** 699 (2000).

24. A. Spitkovsky, Y. Levin, and G. Ushomirsky, Astrophys. J. **566,** 1018 (2002).

25. L. Spitzer, Phys. of Fully Ionized Gases, 2nd rev. ed. (Intersci. Publ., New York, 1962).

26. T. Strohmayer and L. Bildsten, in: Compact Stellar X-ray Sources, Ed. by W.H.G. Lewin and M. van der Klis (Cambridge Univ., Cambridge, 2006), p. 113.

27. V. Suleimanov and J. Poutanen, Mon. Not. R. Astron. Soc. **369,** 2036 (2006).

28. R. Sunyaev and M. Revnivtsev, Astron. Astrophys. **358,** 617 (2000).

29. R.A. Sunyaev and L.G. Titarchuk, Astron. Astrophys. **86,** 121 (1980).

30. R.A. Sunyaev and N.I. Shakura, Sov. Astron. Lett. **12,** 117 (1986).

31. J.L. Tassoul, Theory of Rotating Stars (Princeton Univ., Princeton, 1978; Mir, Moscow, 1982).

32. S. Weinberg, Gravitation and Cosmology: Principles and Applications of the General Theory of Relativity (Wiley, New York, 1972).

33. R. Wijnands and M. van der Klis, Nature **394,** 344 (1998).

34. J.J.M. int Zand, J. Heise, J.M. Muller, et al., Astron. Astrophys. **331,** L25 (1998).